ELSEVIER

Journal of Organometallic Chemistry 529 (1997) 379–385

Journal of Organometallic Chemistry

Cleavage of an acyclic P_5 ligand into $P_4|P_1$ and $P_3|P_2$ molecular building blocks [1]

Otto J. Scherer *, Thomas Mohr, Gotthelf Wolmershäuser [2]

Department of Chemistry, University of Kaiserslautern, 67663 Kaiserslautern, Germany

Received 2 April 1996; accepted 31 May 1996

Abstract

The cothermolysis of $[Cp^*FeP_5]$ (**1**) and $[Cp''Ta(CO)_4]$ (**2**), $Cp'' = C_5H_3{}^tBu_2$ – 1,3, affords the trinuclear cubane-like compounds **3** in the form of the equilibrium mixture $[(Cp^*Fe)(Cp''Ta)_2P_5]$ (**3a**) ⇄ $[(Cp^*Fe)(Cp''Ta)_2(P_4)(P_1)]$ (**3b**) and small amounts of the P_n complexes $[(Cp^*Fe)(Cp''Ta)(P_5)]$ (**4**), $[(Cp''Ta)_3(P_4)(P_2)]$ (**5**), and $[(Cp''Ta)_4(P_3)_2]$ (**6**). Further reaction of **3a,b** with $[Mo(CO)_5(thf)]$ gives exclusively $[(Cp^*Fe)(Cp''Ta)_2(P_5)\{Mo(CO)_5\}]$ (**7**). The skeleton of **7** consists of an FeP_5 six-membered ring capped by two $\{Cp''Ta\}$ fragments. The formal insertion of a $\{Cp''Ta(CO)_2\}$ unit into the intact P_5 chain of **4** provides $[(Cp^*Fe)(Cp''Ta)\{Cp''(OC)_2Ta\}(P_3)(P_2)]$ (**9**), a trinuclear species where the intact P_5 chain of the educt **4** has been cleaved into a P_3 and a P_2 ligand. **7** and **9** have been further characterized by X-ray crystal structure analyses.

Keywords: Iron; Tantalum; Phosphorus; Cage compound; Cluster; Cyclopentadienyl

1. Introduction

Little is known about the selective cleavage of cyclic or acyclic P_n ligands ($n = 3$–6 for example) to ring-opened or smaller fragments (for reviews see Ref. [1]). The cyclo-P_3 ligand of the cationic complexes $[LNi(P_3)]^+$ and $[LCo(P_3Et)]^+$ can be cleaved by reacting it with, for example, $[(Ph_3P)_2Pt(C_2H_4)]$ [2] or $Co^{2+}|L$ ($L = MeC(CH_2PPh_2)_3$) [3]. A strong kite-like distortion ($P_1|P_3$) of the P_4 ring was observed for $[Cp''Co(P_4)\{(CoCp'')_2(\mu\text{-}CO)\}]$ [4]; in contrast, the photolysis of $[Cp''Fe(cyclo\text{-}P_4)\{Fe(CO)_2Cp''\}]$ gives $[(Cp''Fe)_2(P_4)]$ with a P_4 chain [5]. Finally, the cothermolysis of the sandwich complexes $[Cp^*FeP_5]$ and $[Cp''Ta(CO)_4]$ affords $[Cp^*FeP_5TaCp'']$, where one P–P bond of the cyclo-P_5 educt is broken [6]. Interestingly, the P_6 middle deck of the 26 valence-electron triple decker $[(Cp''Nb)_2(P_6)]$, $Cp'' = C_5H_3{}^tBu_2$ – 1,3, is distorted on the way to two P_3 units [7].

2. Results and discussion

The thermolysis of **1** and **2** for 6 h in boiling decalin gives, besides small amounts (ca. 3%) of **4** [6], **5** [8], and **6** [9], in a yield of 42% a mixture of the cubanes **3a,b** with an $FeTa_2P_5$-framework (Scheme 1). Column chromatography followed by recrystallization leads to a black–brown crystalline powder, which is slightly soluble in hexane and readily soluble in toluene.

The equilibrium $[(Cp^*Fe)(Cp''Ta)_2(P_5)]$ (**3a**) ⇄ $[(Cp^*Fe)(Cp''Ta)_2(P_4)(P_1)]$ (**3b**) can be shifted quantitatively to the left side (cubane **3a**) on further coordination of **3a,b** to an $\{Mo(CO)_5\}$ fragment (compound **7**, Scheme 1).

2.1. NMR data of the multinuclear P_5 complexes 3a,b and 7

Table 1 summarizes the ^1H and ^{31}P NMR data of the trinuclear P_5 complexes **3a,b** and **7**.

Temperature dependent ^1H NMR studies [10] on compound **3** in C_6D_6 show that there exists an equilibrium between two isomers (**3a** ⇄ **3b**; 298 K; **3a**:**3b** 1:1.45). Two sets of magnetically different Cp″ ligands, ratio 1:2:18, in a symmetric surrounding are observed

* Corresponding author.

[1] Dedicated to Professor Max Herberhold, Bayreuth, on the occasion of his 60th birthday.

[2] X-ray crystal structure determinations.

PII S0022-328X(96)06557-6

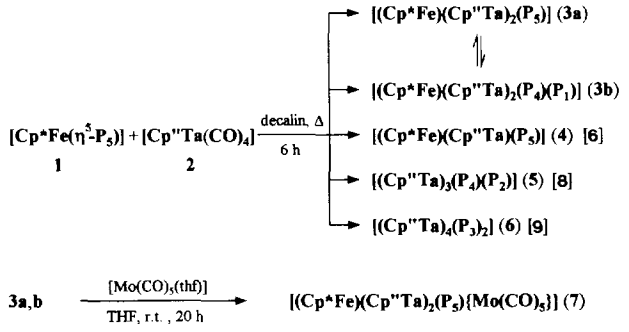

Scheme 1.

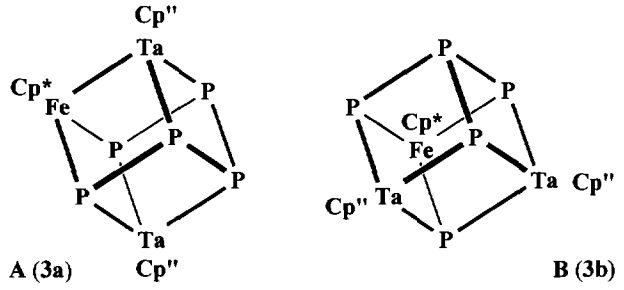

Fig. 1. Proposed molecular structures for the isomers **3a,b**.

for **3a** and **7** ({$Mo(CO)_5$} adduct to **3**). The two Cp″ ligands of **3b** are related through a mirror plane as the only element of symmetry, and thus show a 2:2:2:18:18 splitting pattern. Cp* Fe (15H) gives a singlet for all three complexes (Table 1).

The ^{31}P NMR spectrum of **3a** consists of an AA′MXX′ spin system which is in accordance with a symmetric P_5 chain. The lowest chemical shift (416.3 ppm, Table 1) was found for the 'terminal' P atoms $P_{AA'}$. Interestingly, compounds **3a** and **7** ({$Mo(CO)_5$} adduct to **3a**) do not differ significantly with respect to coupling constants and chemical shifts (Table 1). For **3b** four signal groups can be detected in the ^{31}P NMR spectrum. The four phosphorus atoms form an isotetraphosphide $P_M-P_X(P_N)_2$ unit (P_4 tetrahedron, where three P–P bonds are cleaved, cf. Fig. 1). It is worthwhile mentioning the large chemical shift range of the isomer **3b** (776.8, P_A to −313.3, P_X, Δ = 1090 ppm; **3a**, Δ = 305 ppm, Table 1). P_A is a single phosphorus atom surrounded by two {Cp″Ta} and one {Cp* Fe} fragment. On the basis of the X-ray structure results for compound **7** (Section 2.3) the cubane-like polyhedra **A** (**3a**) and **B** (**3b**) of Fig. 1 are in good agreement with the NMR data.

Less likely is an isomer of **3** with a Ta–Ta edge in the distorted cube. As derived from the NMR data the proposed structure (Fig. 1) with the two Ta atoms in the position of a body diagonal appears most convincing.

3a shows an interesting parallel to $[(Cp^* Ti)_2(\mu\text{-}\eta^{3:3}\text{-}P_6)]$, where a flattened P_6 chair is capped by two {Cp* Ti} fragments [11]. A P_5 resembling **3b** with a P_1 and a tripodal P_4 (trigonal pyramidal) ligand is found in $[(Cp^* Ni)_3(P_4)(P_1)]$, a complex with a distorted Ni_3P_5 cube skeleton [12].

2.2. Cleavage of a P_5 chain ligand into a P_3 and a P_2 fragment

Room temperature reaction of [(Cp* Fe)(Cp″Ta)(P_5)] (**4**) and [Cp″$Ta(CO)_2$(cod)] (**8**) afforded the novel $P_3|P_2$

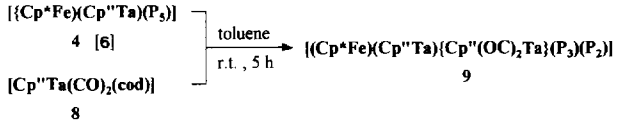

Scheme 2.

Table 1
^1H and ^{31}P NMR data for the P_5 complexes **3a,b** and **7** (in C_6D_6, 298 K, δ in ppm, J in Hz)

[(Cp* Fe)(Cp″Ta)$_2$(P_5)] **3a**	[(Cp* Fe)(Cp″Ta)$_2$(P_4)(P_1)] **3b**	[(Cp* Fe)(Cp″Ta)$_2$(P_5){$Mo(CO)_5$}] **7**
δ ^1H		
6.42 (d, 2H, J = 2.3)	5.74 (m, 2H)	6.79 (m, 1H)
6.21 (m, 1H)	5.07 (m, 2H)	6.25 (d, 2H, J = 2.2)
5.34 (m, 2H)	4.15 (m, 2H)	5.34 (m, 2H)
4.54 (t, 1H, J = 2.3)	1.99 (s, 18H)	5.32 (m, 1H)
1.69 (s, 18H)	1.44 (s, 15H)	1.74 (s, 15H)
1.49 (s, 15H)	1.01 (s, 18H)	1.36 (s, 18H)
1.31 (s, 18H)		1.32 (s, 18H)
δ ^{31}P		
AA′MXX′ spin system	AMN_2X spin system	AA′MXX′ spin system
RMS = 0.40 [a]	RMS = 0.41	RMS = 0.17
416.3 (P_A, m, 2P; ^1J(AX) = −292.2, ^2J(AM) = 36.7)	776.8 (P_A, d, 1P; ^2J(AM) = 11.1)	384.8 (P_A, m, 2P; ^1J(AX) = −312.8, ^2J(AM) = 25.3)
218.6 (P_M, "tt", 1P; ^1J(MX) = −252.6, ^2J(AX′) = −15.5)	332.9 (P_M, dd, 1P; ^1J(MX) = −318.0)	233.5 (PM, "tt", 1P; ^1J(MX) = −284.2, ^2J(AX′) = −7.9)
110.9 (P_X, "ddd", 2P; ^2J(XX′) = 25.9)	267.3 (P_N, d, 2P; ^1J(NX) = −218.3)	142.7 (P_X, "ddd", 2P; ^2J(XX′) = 16.3)
	−313.3 (P_X, dt, 1P)	

[a] RMS = route mean square.

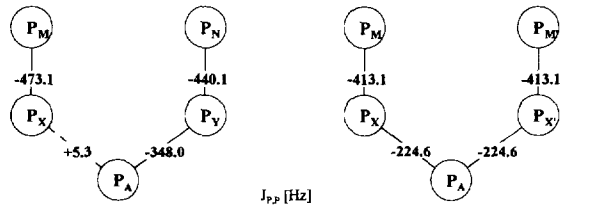

[(Cp*Fe)(Cp"Ta){Cp"(OC)$_2$Ta}(P$_3$)(P$_2$)] **9** [(Cp*Fe)(Cp"Ta)(P$_5$){Ta(CO)$_3$Cp"}] **10**

Scheme 3. Proposed arrangement and notation as well as J(P–P) coupling constants for the $P_3|P_2$ ligands of complex **9** in comparison with the symmetric P_5 unit of **10**.

complex **9** (Scheme 2) in high yield and small amounts of [(Cp* Fe)(Cp"Ta)(μ_3-P$_5$){Ta(CO)$_3$Cp"}] (**10**) ({Ta(CO)$_3$Cp"} adduct to **4**) and [(Cp* Fe)(Cp"Ta)-{Cp"(OC)$_2$Ta}(P$_3$)(P$_2$){Ta(CO)$_3$Cp"}] (**11**) (adduct to **9**).

The complexes **9–11** could be separated chromatographically. **9** forms a brown powder which is slightly soluble in hexane and readily soluble in toluene. It can be recrystallized from n-hexane at ca. −78 °C.

2.2.1. Discussion of the ^{1}H and ^{31}P NMR data of the $P_3|P_2$ complex 9

In the ^{1}H NMR spectrum one observes a singlet for the {Cp* Fe} ligand and two different sets (1:1:1:9:9) for each {Cp"Ta} group. This pattern as well as the five different ^{31}P NMR signals (AMNXY spin system) reflect the asymmetric FeTa$_2$P$_5$ skeleton of **9**. The P_5 part can be divided into a P_3 unit (P_A–P_Y–P_N) and a P_2 fragment (P_M–P_X).

The proposed connectivity of the phosphorus atoms (Scheme 3) has been derived from the ^{31}P NMR data of **9**, comparing it with [(Cp* Fe)(Cp"Ta)(μ_3-P$_5$){Ta(CO)$_3$Cp"}] (**10**), a complex with an intact P_5 chain. **9** can also be formed by photochemical decarbonylation of **10** and formal insertion of the {Cp"(OC)$_2$Ta} fragment into a P–P bond.

The ^1J(P–P) coupling constants show meaningful trends. For example, $^1J(P_N–P_Y)$ of **9** (−440.1) and $^1J(P_M–P_X)$ of **10** are in a comparable range. The larger value of $^1J(P_M–P_X)$ in **9** is in favour of a higher multiple-bond character of its P_2 ligand. Less informative are the long-range coupling constants (4.6 to 25.8 Hz, Table 2). All attempts failed to obtain further information about the coordination geometry of the $P_5(P_3|P_2)$ ligand by ^{31}P^{31}P-COSY-45-NMR experiments.

2.3. Molecular structures of the complexes [(Cp* Fe)(Cp"Ta)$_2$(P$_5$){Mo(CO)$_5$}] (7) and [(Cp* Fe)(Cp"Ta){Cp"(OC)$_2$Ta}(P$_3$)(P$_2$)] (9)

Selected bond lengths (Å) and angles (°) are compiled in Table 3 (see also Section 3).

Fig. 2 shows the molecular structure of complex **7** with a P_5 chain ligand, Fig. 3 illustrates the molecular structure of compound **9** with a $P_3|P_2$ subunit. In Fig. 4 the FeTaP$_5$ skeleton of [{Cp* Fe}{Cp"Ta}(P$_5$)] (**4**) [6] is shown for comparison.

2.3.1. [(Cp* Fe)(Cp"Ta)$_2$(P$_5$){Mo(CO)$_5$}] (7)

The most interesting part of complex **7** is an FeP$_5$ ring with flattened chair conformation capped by a {Cp"Ta} fragment on each side (Fig. 2). The Ta1 · · · Ta2 distance in the distorted cube is 3.038(1) Å. The P_5 part of the six-membered ring shows a striking parallel to the analogous ligand in [(Cp* Fe)(Cp"Ta)(P$_5$)] (**4**) [6] (Table 4, Fig. 4). The faces of the cube are nearly parallel to each other (distortion 0.2 to 1.0°). Their sum of bond angles varies between 356.5 and 359.4°.

Besides the short (**7**, 2.22 Å|**4**, 2.15 Å) and long (2.28 Å|2.27 Å) P–P bonds, the P1 · · · P5 distance (3.54 Å|3.60 Å) as well as the Ta–Ta distances (2.984 Å|2.85 Å) of **7** and **4** do not differ significantly (Table 4). Going from the FeTaP$_5$ skeleton of **4** (Fig. 4) to that of complex **7** (Fig. 2), formally, the iron atom migrates to the P1 · · · P5 edge followed by a capping reaction of the Ta2 atom. Afterwards, Ta1 is also in a position to cap the FeP$_5$ ring (Fig. 2). As a consequence of these structural changes the most important differences between **7** and **4** are found for P2 · · · P4 (**7**, 3.81 Å|**4**, 2.80 Å) and the folding angle of the P_5 'envelope' part (**7**, 134.5 Å|**4**, 108.8°, Table 4). The mean

Table 2
^{1}H and ^{31}P NMR data of [(Cp* Fe)(Cp"Ta){Cp"(OC)$_2$Ta}(P$_3$)(P$_2$)] (**9**) (in C$_6$D$_6$, 298 K, δ in ppm, J in Hz)

δ ^{1}H	δ ^{31}P
5.88 (m, 1H), 1.40 (s, 9H)	AMNXY spin system
5.25 (m, 1H), 1.38 (s, 9H)	689.6 (P_A, "dd", 1P; ^1J(AY) = −348.0, ^2J(AN) = 25.8
5.20 (m, 1H), 1.18 (s, 9H)	299.4 (P_M, "d", 1P; ^1J(MX) = −473.1, J(AM) = 4.6
4.97 (m, 1H), 1.14 (s, 9H)	284.8 (P_N, "dd", 1P; ^1J(NY) = −440.1, J(AX) = 5.3
4.80 (m, 1H)	191.6 (P_X, "d", 1P; J(MN) = 5.9, J(MY) = 10.2
4.72 (m, 1H)	69.2 (P_Y, "dd", 1P; J(NX) = 14.6, J(XY) = 7.2
1.71 (s, 15H)	RMS (route mean square) 0.26

Table 3
Selected bond lengths (Å) and angles (°) for the complexes **7** and **9**

[(Cp* Fe)(Cp″Ta)$_2$(P$_5$){Mo(CO)$_5$}] (**7**)				[(Cp* Fe)(Cp″Ta){Cp″(OC)$_2$Ta}(P$_3$)(P$_2$)] (**9**)			
Fe–Ta2	2.458(2)	Fe–P1	2.225(4)	Fe–P1	2.380(3)	Fe–P2	2.256(3)
Fe–P5	2.201(5)	Ta1–P1	2.431(4)	Fe–P4	2.259(2)	Fe–P5	2.359(3)
Ta1–P3	2.395(4)	Ta1–P5	2.429(5)	Ta2–P2	2.501(2)	Ta2–P3	2.483(2)
Ta2–P2	2.473(4)	Ta2–P4	2.465(4)	Ta1–P1	2.481(2)	Ta1–P3	2.547(2)
P1–P2	2.220(6)	P2–P3	2.279(6)	Ta1–P5	2.435(2)	Ta1–Fe	2.892(1)
P3–P4	2.284(6)	P4–P5	2.216(6)	P1–P2	2.096(3)	P4–P5	2.132(3)
Ta1 · · · Ta2	3.038(1)	Ta1 · · · Fe	2.984(2)	P3–P4	2.231(3)	Ta1 · · · P2	2.600(2)
Ta1 · · · P2	2.829(4)	Ta1 · · · P4	2.798(4)	Ta1 · · · P4	2.674(2)	Ta1 · · · Ta2	3.278(1)
Ta2 · · · P1	2.792(4)	Ta2 · · · P3	2.776(4)	P2 · · · P3	3.31	P2 · · · P4	3.11
Ta2 · · · P5	2.777(4)	Mo–P3	2.539(4)	P1 · · · P5	3.41		
Fe–Cp$^*_{(centr.)}$	1.764			Fe–Cp$^*_{(centr.)}$	1.748	Ta1–Cp″$_{(centr.)}$	2.131
Ta1–Cp″$_{(centr.)}$	2.093	Ta2–Cp″$_{(centr.)}$	2.104	Ta2–Cp″$_{(centr.)}$	2.093		
P1–Fe–P5	106.1(2)	P1–Fe–Ta2	73.00(12)	P2–Fe–P4	87.14(9)	P2–Fe–P5	112.72(9)
P5–Fe–Ta2	72.93(12)	P1–Ta1–P3	98.76(14)	P4–Fe–P5	54.93(9)	P2–FeP1	53.69(9)
P1–Ta1–P5	93.36(14)	P3–Ta1–P5	99.39(13)	P4–Fe–P1	115.53(9)	P5–Fe–P1	92.11(9)
Fe–Ta2–P4	98.56(11)	Fe–Ta2–P2	98.86(11)	P2–P1–Fe	60.13(9)	P2–P1–Ta1	68.63(8)
P2–Ta2–P4	101.06(14)	Fe–P1–Ta1	79.59(14)	Fe–P1–Ta1	72.99(7)	P1–P2–Fe	66.18(10)
Fe–P1–P2	114.9(2)	Ta1–P1–P2	74.8(2)	P1–P2–Ta2	130.33(12)	Fe–P2–Ta2	133.70(10)
P1–P2–Ta2	72.8(2)	P3–P2–Ta2	71.4(2)	Ta1–P3–P4	67.69(8)	Ta2–P3–P4	111.41(10)
P1–P2–P3	109.0(2)	P2–P3–P4	113.3(2)	P3–P4–P5	113.99(13)	Ta1–P3–Ta2	81.33(6)
P2–P3–Ta1	74.4(2)	P4–P3–Ta1	73.4(2)	Fe–P4–P3	119.47(12)	Fe–P4–P5	64.91(9)
P3–P4–P5	109.7(2)	P5–P4–Ta2	72.6(2)	Ta1–P5–P4	71.32(9)	Fe–P5–Ta1	74.19(7)
P3–P4–Ta2	71.4(2)	Fe–P5–Ta1	80.08(14)	P4–P5–Fe	60.16(9)		
P4–P5–Ta1	73.9(2)	P4–P5–Fe	115.3(2)				

value of the P–P bond lengths (2.25 Å for **7**) is in good agreement with the 2.24 Å in [(Cp* Ti)$_2$(μ-$\eta^{3:3}$-P$_6$)] with the same structural features; namely a P$_6$ chain capped by two Cp* Ti fragments [11]. The Ti · · · Ti distance (3.19 Å) is slightly longer than the Ta · · · Ta of **7** (3.04 Å).

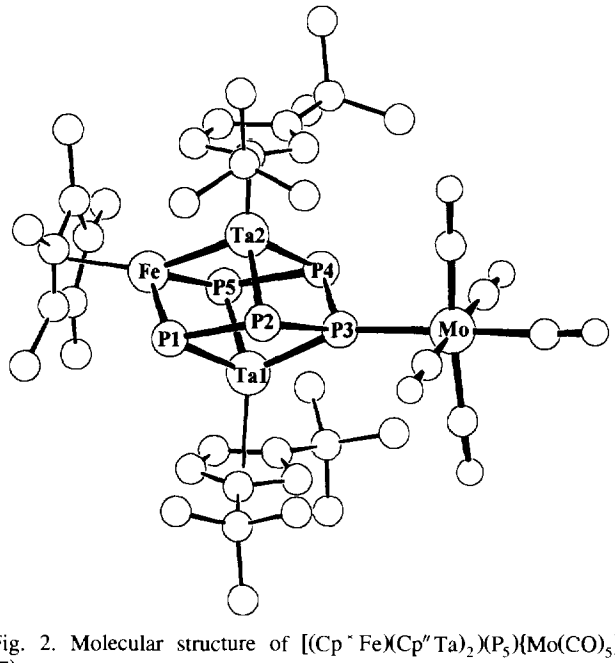

Fig. 2. Molecular structure of [(Cp* Fe)(Cp″Ta)$_2$)(P$_5$){Mo(CO)$_5$}] (**7**).

According to the Wade/Mingos electron-counting rules [13], the core of **7** possesses 58 valence electrons (VE); an electron deficiency of 12 (70 VE-58). It is difficult to answer the question whether there exist metal–metal bonds between Fe · · · Ta1 (2.984(2) Å) and Ta1 · · · Ta2 (3.038(1) Å). For example, the Ta–Ta distance in the dinuclear complex [Cp* Ta(CO)$_2$(μ-Cl)]$_2$ is 3.062(1) Å [14] compared with the sum of the Fe/Ta covalent radii (2.50 Å); the distance Fe–Ta2 (2.458(2) Å) (Table 3) in **7** is only slightly shortened. Formally, the FeTa$_2$P$_5$ framework of **7** can be regarded as an isosce-

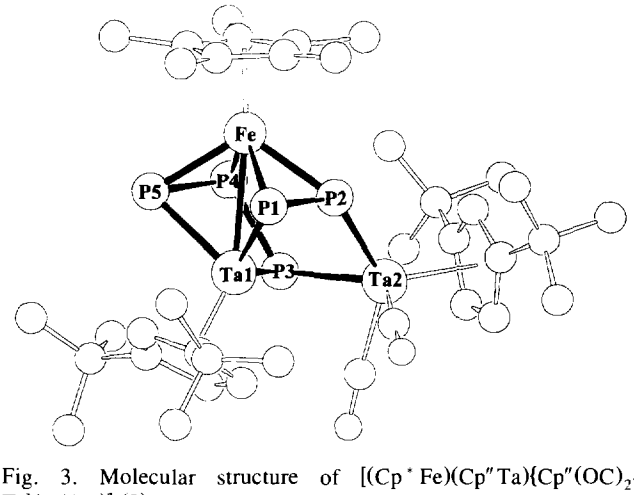

Fig. 3. Molecular structure of [(Cp* Fe)(Cp″Ta){Cp″(OC)$_2$-Ta}(P$_3$)(P$_2$)] (**9**).

Table 4
Comparable bond lengths (Å) and angles (°) for the complexes **7** and **4**

[(Cp* Fe)(Cp″Ta)$_2$(P$_5$){Mo(CO)$_5$}] (**7**)		[(Cp* Fe)(Cp″Ta)(P$_5$)] (**4**) [6]
P1–P2|P4–P5	2.221 [a]	2.151 [a]
P2–P3|P3–P4	2.280 [a]	2.268 [a]
P1 · · · P5	3.537	3.602
P2 · · · P4	3.807	2.804
Fe · · · Ta1|Fe–Ta	2.984	2.854
P$_5$ envelope folding angle	134.5	108.8

[a] Mean value.

les $FeTa_2$ triangle which is nearly symmetrically bridged by a P_5 chain (Fig. 2).

2.4. [(Cp* Fe)(Cp″Ta){Cp″(OC)$_2$Ta}(P$_3$)(P$_2$)] (9)

The $FeTa_2P_3P_2$ skeleton of **9** (cf. Fig. 3) and the $FeTaP_5$ core of **4** (Fig. 4) show remarkable parallels as well as differences. As expected, the P1–P2 bond of the P_2 ligand shortens to 2.096(3) Å (Table 3), whereas in **4** [6] 2.150(2) Å (Table 4) was found for the P1–P2 distance of the P_5 chain.

The cleaved P2 · · · P3 bond (3.31 Å) in **9** differs distinctly from d(P2–P3) = 2.271(2) Å in the intact P_5 chain of **4**. Despite the formal insertion of a {Cp″Ta(CO)$_2$} fragment into the P2–P3 bond of **4** (Figs. 3 and 4), the envelope-like conformation of the five P atoms is comparable for **9** and **4**. Going from **4** (acyclic P_5 ligand) to **9** (P_3|P_2 ligands) the folding angle P1,2,4,5|P2,3,4 expands from 108.8° in **4** to 115.1° in **9**. Interestingly, for the P_2 unit of complex **9** the rare μ_3-$\eta^{2:1:1}$-E_2 (E = P, As) coordination mode was found; it has been realized for the first time in [(Cp* Co)$_3$(μ-$\eta^{2:2}$-As$_2$)(μ_3-$\eta^{2:1:1}$-As$_2$)$_2$] [15] (cf. [(Cp* Co)$_3$P$_6$] [16]). The most intriguing structural part of complex **9** is the acyclic P_3 ligand. Nearly the same trend in P–P bond lengths (**9**, P3–P4 = 2.231(3), P4–P5 = 2.132(3) Å) was found in [(Cp* Mo)$_2$(μ-$\eta^{2:2}$-PS)(μ_3-$\eta^{3:3:1}$-P$_3$){Cr(CO)$_5$}] (**12**) [17] (d(P$_3$) = 2.286(6) Å|2.109(7) Å), the only other compound where, to the best of our knowledge, an acyclic, substituent-free P_3 ligand has been realized. The PPP bond angles differ by 6.2° (**9**, 113.99(13)°; **12**, 107.8(2)°).

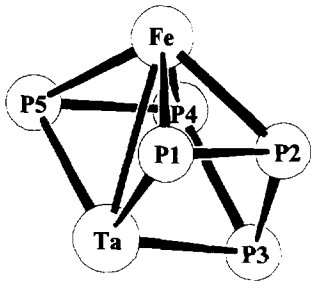

Fig. 4. $FeTaP_5$ skeleton of [(Cp* Fe)(Cp″Ta)P$_5$] (**4**) [6]. Cp* and Cp″ ligands have been omitted.

The coordination mode of the acyclic P_3 ligand in complex **9** (Fig. 3) is very unusual. Besides an η^2 (P4–P5), one terminal (P5–Ta1) and one bridging (P3–Ta1,2) coordination can be derived. The ligand should be described as μ_3-$\eta^{2:1:1:1}$-P_3. Whereas Fe–Ta1 = 2.892(1) Å differs only slightly from the comparable Fe–Ta bond length (2.854(1) Å) in **4** [6], the distances Ta1 · · · P2 = 2.600(2) and Ta1 · · · P4 = 2.674(2) Å (face diagonals) are distinctly longer in **4** (mean value 2.75 Å, cf. Figs. 3 and 4) than in **9**.

A further interesting parallel to **9** was found for the dinuclear complex [{(tripod)Co}$_2$(μ-$\eta^{3:3}$-P$_3$Et)][BF$_4$]$_2$, where for the first time the coordinative stabilization of EtP_3, the all-phosphorus analogue of EtN_3 (ethyl azide), has been realized [3]. Ab initio calculations on P_3^- (16 VE), the phosphorus analogue of the azide ion N_3^- (16 VE), show that the bent P_3^- isomer differs energetically only slightly from the linear one [18].

3. Experimental details

All experiments were carried out under an argon atmosphere in dry solvents. [Cp* FeP$_5$] (**1**) [19], [Cp″Ta(CO)$_4$] (**2**) [20] and [(Cp* Fe)(Cp″Ta)(P$_5$)] (**4**) [6] were prepared as described in the literature. ^{1}H and ^{31}P NMR spectra were measured on a Bruker AC 200 or AMX 400 (^{1}H: C_6D_5H = 7.20 ppm or $C_6D_5CD_2H$ = 2.30 ppm as internal standard; ^{31}P: 85% H_3PO_4 as external standard). Simulation and iteration of the spectra were carried out with PERCH-NMR software [21]. IR spectra were recorded on a Perkin–Elmer 881. UV-irradiation: 150 W Hg high-pressure lamp, TQ 150, Heraeus Quarzlampen GmbH, Hanau.

3.1. Syntheses of the complexes 3a,b, 4, 5 and 6

1.655 g (3.519 mmol) **2** and 0.409 g (1.182 mmol) **1**, each dissolved in ca. 5 ml decalin, were added to a 250 ml three-necked flask filled with 120 ml decalin and heated to reflux with stirring. During the reaction (6 h) the colour changed from yellow–green to black–brown. After evaporation of the solvent under oil-pump vacuum the residue was dissolved in ca. 10 ml dichloromethane,

ca. 1 g of silica gel was added and the mixture was concentrated until it was free-flowing. Column chromatography (column 27 × 1.5 cm^2, SiO_2, petroleum ether) afforded, with petroleum ether|toluene (25:1), 161 mg (10%) unreacted yellow **2**. Afterwards (mixture 15:1), 30 mg (2% based on **1**) $[(Cp''Ta)_4(P_3)_2]$ (**6**) [9] was eluted as a grey–violet zone. Petrolether|toluene (10:1) gave 29 mg (4% based on **1**) olive-green $[(Cp''Fe)(Cp''Ta)(P_5)]$ (**4**) [6], followed by an 8:1 mixture which provides 41 mg (3% based on **1**) green $[Cp''Ta)_3(P_4)(P_2)]$ (**5**) [8]. Finally, petrolether|toluene (5:1 to 2:1) eluted 525 mg (42% based on **1**) black–brown equilibrium mixture $[(Cp^*Fe)(Cp''Ta)_2P_5]$ (**3a,b**), which was recrystallized from a saturated n-hexane|dichloromethane solution at −78 °C. Anal. Found: C, 39.61; H, 5.32. $C_{36}H_{57}FeP_5Ta_2$ Calc.: C, 40.70; H, 5.41%.

3.2. Synthesis of $[(Cp^*Fe)(Cp''Ta)_2(P_5)\{Mo(CO)_5\}]$ (7)

A solution of $[Mo(CO)_5(thf)]$, prepared from 263 mg (1.00 mmol) $[Mo(CO)_6]$ by irradiation (30 min in a UV apparatus) in 70 ml THF, was added at room temperature with stirring to a solution of 259 mg (0.244 mmol) **3a,b** in ca. 10 ml THF (100 ml flask) and stirred for 20 h at room temperature. Afterwards, the solvent was evaporated under oil-pump vacuum, the residue was dissolved in ca. 5 ml dichloromethane, ca. 1 g of silica gel was added, and the mixture was concentrated until it was free-flowing. Column chromatography (column 20 × 2 cm^2, SiO_2, petroleum ether) gave, with petroleum ether|toluene (20:1), a small yellow zone ($[Mo(CO)_6]$). Petroleum ether|toluene (5:1) eluted 149 mg (47% based on **3a,b**) green–brown **7**, which was recrystallized from n-hexane at −78 °C. Anal. Found: C, 36.93; H, 4.41. $C_{41}H_{57}MoO_5P_5Ta_2$ Calc.: C, 37.93; H, 4.42%.

3.3. Synthesis of $[(Cp^*Fe)(Cp''Ta)\{Cp''(OC)_2Ta\}(P_3)(P_2)]$ (9)

3.3.1. $[Cp''Ta(CO)_2(cod)]$ (8)

313 mg (0.666 mmol) $[Cp''Ta(CO)_4]$ (**2**) and 704 mg (6.47 mmol) cyclooctadiene (COD), dissolved in 50 ml toluene, were irradiated (UV apparatus) in a 70 ml apparatus. After 50 min IR spectroscopically exclusively the CO bands of **8**, which was handled only in solution, could be detected.

Starting with 299 mg (0.618 mmol) **2** and 704 mg (6.47 mmol = 0.8 ml) COD in ca. 50 ml toluene its cophotolysis provided a solution of **8** (IR: ν(CO) = 1974(s), 1866(s)). Afterwards, 220 mg (0.312 mmol) of $[(Cp^*Fe)(Cp''Ta)(P_5)]$ (**4**) in 5 ml toluene was added and this solution was stirred for ca. 5 h until the IR-CO bands of **9** (1954(s), 1895(s)) attained a maximum. After evaporation of the solvents under oil-pump vacuum the residue was dissolved in ca. 10 ml dichloromethane, ca. 1 g of silylated silica gel was added, and the mixture was concentrated until it was free-flowing. Column chromatography (column 28 × 1.5 cm^2, SiO_2, petroleum ether), starting with petroleum ether|toluene (20:1), gave, with a 3:1 mixture, traces of **4**, followed by 21 mg (6% based on **4**) orange–brown mono-adduct $[(Cp^*Fe)(Cp''Ta)(\mu_3\text{-}P_5)\{Ta(CO)_3Cp''\}]$ (**10**) [10]. Further elution led to 19 mg (4% based on **4**) dark-grey $[(Cp^*Fe)(Cp''Ta)\{Cp''(OC)_2Ta\}(P_3)(P_2)\{Ta(CO)_3Cp''\}]$ (**11**) [10], the $\{Ta(CO)_3Cp''\}$ adduct of **9**. A petroleum ether|toluene mixture of 2:1 eluted 282 mg (81% based on **4**) brown **9**, which can be recrystallized from n-hexane at −78 °C. Anal. Found: C, 40.52; H, 5.21. $C_{38}H_{57}FeO_2P_5Ta_2$ Calc.: C, 40.81; H, 5.14%.

3.4. X-ray crystal structure determinations of 7 and 9

Crystal data for **7** [**9**]: $C_{41}H_{57}FeMoO_5P_5Ta_2$ [$C_{38}H_{57}FeO_2P_5Ta_2$]; M_r = 1298.4 [1118.4]; monoclinic; space group $P2_1/c$ [$P2_1/n$]; a = 12.607(3) [12.343(2) Å], b = 17.0479(10) [21.987(2) Å], c = 23.126(5) [15.6140(10) Å]; β = 102.469(10) [99.000(10)°]; V = 4853.1(14) [4185.2(8) Å^3]; Z = 4; D_c = 1.777 [1.775 g cm^{-3}]; μ(Mo Kα) = 52.43 [57.80 cm^{-1}]; measured reflections 11293 [11453], independent reflections 10505 [9579], R(int) = 0.0615 [0.0477], refined parameters 518 [455]; diffractometers Enraf–Nonius CAD4 [Siemens P4]; T 293 [183 K]; θ range 2.04–26.94° [2.17–27.50°]; R_1 = 0.1629 [0.1041], wR_2 = 0.1482 [0.0864] (all data, refinement according to F^2). Structure solution by direct methods, SHELXS-86 [SIR 92].

Further details of the X-ray structure determinations may be obtained from the Fachinformationszentrum Karlsruhe GmbH, D-76344 Eggenstein-Leopoldshafen, Germany on quoting the depository numbers CSD-405320 and CSD-405321, the names of the authors and the journal citation.

Acknowledgements

We thank the Fonds der Chemischen Industrie and the Graduiertenkolleg 'Phosphorus Chemistry as a Link Between Different Chemical Disciplines' for financial support. The help of Dr. K. Öfele, TU München, in preparing $[Cp''Ta(CO)_4]$ is gratefully acknowledged.

References

[1] O.J. Scherer, *Angew. Chem.*, *102* (1990) 1137; *Angew. Chem., Int. Ed. Engl.*, *29* (1990) 1104; M. Scheer and E. Herrmann, *Z. Chem.*, *30* (1990) 41.

[2] M. Di Vaira, P. Stoppioni and M. Peruzzini, *Polyhedron*, *6* (1987) 35.

[3] A. Barth, G. Huttner, M. Fritz and L. Zsolnai, *Angew. Chem., 102* (1990) 956; *Angew. Chem., Int. Ed. Engl., 29* (1990) 929.
[4] M. Scheer, U. Becker, M.H. Chisholm, J.C. Huffman, F. Lemoigno and O. Eisenstein, *Inorg. Chem., 34* (1995) 3117.
[5] O.J. Scherer, G. Schwarz and G. Wolmershäuser, *Z. Anorg. Allg. Chem., 622* (1996) 951.
[6] M. Detzel, T. Mohr, O.J. Scherer and G. Wolmershäuser, *Angew. Chem., 106* (1994) 1142; *Angew. Chem., Int. Ed. Engl., 33* (1994) 1110.
[7] A.C. Reddy, E.D. Jemmis, O.J. Scherer, R. Winter, G. Heckmann and G. Wolmershäuser, *Organometallics, 11* (1992) 3894.
[8] O.J. Scherer, R. Winter and G. Wolmershäuser, *J. Chem. Soc., Chem. Commun.*, (1993) 313.
[9] T. Mohr, O.J. Scherer and G. Wolmershäuser, in preparation; cf. $[\{CpV\}_4(P_3)_2]$ M. Herberhold, G. Frohmader and W. Milius, *Phosphorus, Sulfur, and Silicon, 93/94* (1994) 205.
[10] T. Mohr, *Thesis*, University of Kaiserslautern, 1996 (unpublished).
[11] O.J. Scherer, H. Swarowsky, G. Wolmershäuser, W. Kaim and S. Kohlmann, *Angew. Chem., 99* (1987) 1178; *Angew. Chem., Int. Ed. Engl., 26* (1987) 1153.
[12] O.J. Scherer, J. Braun and G. Wolmershäuser, *Chem. Ber., 123* (1990) 471.
[13] K. Wade, *Adv. Inorg. Chem., 18* (1976) 1; D.M.P. Mingos and R.L. Johnston, *Struct. Bond., 68* (1987) 29.
[14] D. Kwon, J. Real, M.D. Curtis, A. Rheingold and B.S. Haggerty, *Organometallics, 10* (1991) 143.
[15] O.J. Scherer, K. Pfeiffer, G. Heckmann and G. Wolmershäuser, *J. Organomet. Chem., 425* (1992) 141.
[16] R. Ahlrichs, D. Fenske, K. Fromm, H. Krautscheid, U. Krautscheid and O. Treutler, *Chem. Eur. J., 2* (1996) 237.
[17] H. Brunner, U. Klement, W. Meier, J. Wachter, O. Serhadle and M.L. Ziegler, *J. Organomet. Chem., 335* (1987) 339.
[18] J.K. Burdett and C.J. Marsden, *New J. Chem., 12* (1988) 797.
[19] M. Detzel, G. Friedrich, O.J. Scherer and G. Wolmershäuser, *Angew. Chem., 107* (1995) 1454; *Angew. Chem., Int. Ed. Engl., 34* (1995) 1321.
[20] O.J. Scherer, R. Winter and G. Wolmershäuser, *Z. Anorg. Allg. Chem., 619* (1993) 827.
[21] R. Laatikainen and M. Niemitz, *PERCH-NMR Software*, University of Kuopio, Finland, 1995.